Research Article

Gamma-radiation induced synthesis of spinel Co_3O_4 nanoparticles

Jérémie L. Muswema[1] · Gracien B. Ekoko[1] · Joseph K.-K. Lobo[1] · Omer M. Mvele[1] · Hercule M. Kalele[1] · Antoine K. Mbongo[1] · Gérard N. Mata[1]

Abstract
Gamma irradiation method has been applied to produce paramagnetic spherically shaped single crystals tricobalt tetraoxide (Co_3O_4) nanoparticles from cobalt oxyhydroxide sols, in alkaline medium pH ~ 12. The present investigation has proven the efficiency of gamma rays in inducing changes in structure and morphology of the sols prepared before irradiation. Characterization techniques so far discussed in this study revealed that the sol product prepared before irradiation corresponded to the standard cobalt(III) oxyhydroxide, CoO(OH), which, under gamma irradiation, was transformed to tricobalt tetraoxide, Co_3O_4, with an average particle size of ~ 30–45 nm.

Keywords Tricobalt tetraoxide · Paramagnetic · Nanoparticles · γ-irradiation

1 Introduction

Nanotechnology is the science of production, manipulation and use of materials at subatomic level to produce novel products and processes. In recent years, noble metal oxide nanoparticles have been the subject of focused research due to their unique electronic, optical, mechanical, magnetic and chemical properties that are significantly different from those of bulk counterpart [1–3].

The tricobalt tetraoxide is a magnetic semiconductor. It crystallizes in a spinel structure which contains cobalt ions in two different oxidation states, the Co^{3+} ions occupying the octahedral sites, and a Co^{2+} ions occupying tetrahedral sites with the oxygen ions forming a close-packed face centered cubic lattice [4–7].

Despite these important technological applications, the amount of available information on Co_3O_4 is still limited. Cobalt oxide is an important multifunctional material and it has three well-known polymorphs, the cobaltous oxide (CoO), the cobaltic oxide (Co_2O_3) and the tricobalt tetraoxide (Co_3O_4). Compared to the other two polymorphs, Co_3O_4 has attracted great interest owing to its potential application in energy storage [8], efficient catalysts in a lot of heterogeneous chemical processes [9], electronic devices [10], solar absorber [11], lithium-ion battery as electrode material [9], supercapacitor [12, 13], gas sensor [14] and thermal stability [15].

Cobalt oxide nanoparticles have been synthesized by different techniques including sol–gel techniques [16], thermal annealing synthesis [17], co-precipitation method [18], microwave-assisted [19], reverse micelles [20], spray pyrolysis [21], sonochemical method [22], microwave heating [23], ionic liquid assisted method [24], polyol method [25] and a nonaqueous route [26] and gamma-radiolysis-assisted cobalt oxide nanoparticle formation [27].

These methods are either complex or require chemically harsh conditions and/or high processing temperatures for the synthesis of nanoscale crystalline Co_3O_4 particles. Gamma irradiation method is a promising new technique which avoids the need for chemical and thermal extreme conditions for the synthesis of Co_3O_4 nanoparticles. This technique could be hopefully used to simplify the experimental process, which is an interesting strategy to construct new catalysts [1–8].

✉ Jérémie L. Muswema, jeremie.muswem@unikin.ac.cd | [1]Department of Chemistry, Faculty of Science, University of Kinshasa, P.O. Box 190, KIN XI, Democratic Republic of the Congo.

SN Applied Sciences (2019) 1:333 | https://doi.org/10.1007/s42452-019-0342-6

Received: 17 December 2018 / Accepted: 5 March 2019

Published online: 12 March 2019

It is well known that under γ-irradiation, in pure water, the primary radiolysis products continue to react with each other to form secondary products such as $^{\cdot}HO_2$, O_2, $O_2^{\cdot-}$, and eventually the stable products H_2, O_2 and H_2O_2. The concentrations of the radiolysis products depend on the radiation energy absorption rate, solution pH, and the temperature [28, 29].

The radiolysis products are highly redox active and include both oxidizing ($HO^{\cdot}$,H_2O_2 and O_2) and reducing ($H^{\cdot}$, e^-_{aq} and $O_2^{\cdot-}$) species. These species can readily interact with dissolved transition metal ions to change their oxidation states. Conversion of dissolved metal species to oxidation states with low solubilities can lead to condensation and formation of oxide particles.

In our previous works, γ-irradiation method has been applied to produce magnetic Fe_3O_4 nanorod particles and Fe_2O_3 in alkaline medium by controlling the pH, which has an influence on the morphology of fabricated iron oxides [30–32].

In the present investigation, we report on γ-irradiation as a facile method to produce monodispersed Co_3O_4 nanopowders, prepared by irradiating the starting aerated sol of cobalt oxyhydroxide, CoO(OH), prepared at pH ~ 12.0.

2 Experimental details

2.1 Sample preparation procedure

All reagents for making nanostructured Co_3O_4 were of high-purity analytical grade and were used as received: cobalt(II) chloride hexahydrate, [$CoCl_2{\cdot}6H_2O$] as Co^{2+} source, distilled water, isopropyl alcohol, [$(CH_3)_2CHOH$], anhydrous sodium hydroxide, [NaOH], polyvinyl alcohol [PVA] and ammonium buffers.

(a) Preparation of CoO(OH) before γ-irradiation

An experiment was setup before the prepared sols to be γ-irradiated. Sols of CoO(OH) were prepared from $CoCl_2{\cdot}6H_2O$ to form a Co $(OH)_2$ precipitate. An anhydrous sodium hydroxide was added to aqueous solution of 0.04 mol L^{-1} $CoCl_2{\cdot}6H_2O$ under constant stirring with a magnetic stirrer until the pH of the suspension increased to about 9. Ammonium buffers were ultimately chosen to avoid the irreversible precipitation of parasitic cobalt salts, as occurs, for instance, in buffers containing carbonates or phosphates. The reddish coloured sols constituted of cobaltous hydroxide, [$Co(OH)_2$] were prepared at pH about 9.

Concentrated solution of anhydrous sodium hydroxide was added drop wise into the solutions by stirring the solutions continuously until brown solution was obtained at pH about 12, which expect the formation of $Co(OH)_3$. The precipitate was separated from the mother solution by repeating filtration and centrifugation and then was washed by ethyl alcohol to eliminate soluble salts and/or chloride ions and cobalt oxyhydroxide, CoO(OH) was obtained 2 h later afterwards from $Co(OH)_3$ in air. These pH values were chosen based on the solubilities of Co(II) and Co(III) species [33].

The obtained precipitates were dried in vacuum oven at 60 °C for 4 h and analyzed by XRD and their morphology was observed by TEM.

(b) γ-irradiation preparation of Co_3O_4 nanoparticles

On the other hand, when the sols CoO(OH) were formed at pH about 12, 20 g were mixed with sodium carbonate (0.01 mol L^{-1}) to keep the pH values constant at about 12. In order to improve the production yield of nanoparticles, isopropyl alcohol (3.0 mol L^{-1}) was firstly poured into the solutions to act as scavenger for oxidative radicals OH·, produced during the radiolysis of water under gamma irradiation. To prevent the small particles from coming into close contact and undergoing further aggregation, an organic surfactant, polyvinyl alcohol, PVA (1%, w/w) was then added in the solution.

The prepared sols were irradiated in the field of a ^{60}Co γ ray source of 1.2025×10^{16} Bq (325,000 Ci). The absorbed dose of irradiation was 30 kGy with a dose rate of about 0.25 kGy h^{-1}. After γ-irradiation, black coloured precipitates were obtained and they were separated by washing with distilled water and absolute alcohol, in order to remove the by-products, and were finally dried in a vacuum oven at 60 °C for 4 h. The black precipitate constituted of pure Co_3O_4 was obtained and analyzed.

2.2 Characterization techniques

All reagents and solvents for synthesis and analysis were commercially available and used as received without further purifications. The structure and the phase identification of the prepared materials was carried out on X-ray powder diffraction (XRD) patterns, using a D/MAX-2550 X-ray diffractometer with Cu-Kα radiation (λ = 1.54056 Å) with a nickel filter (Rigaku Co., Japan). The crystalline sizes were calculated by using the Debye–Scherrer formula. The chemical bondings in Co_3O_4 were recorded by Fourier transform infrared spectra (SHIMADZU Spectrophotometer) using KBr pellet technique in the range from 4000 to 400 cm^{-1} (spectral resolution at 4 cm^{-1} and number of scans at 20). The surface morphology, size of particles and elemental compositions of Co_3O_4 were carried out by field emission scanning electron microscopy (FE-SEM; JEOL JSM-6700F) well equipped with an energy dispersive

X-ray (EDAX) spectrophotometer and operated at 20 kV. The chemical bonding on the composite surface was studied using X-ray photoelectron spectroscopy (XPS), which was performed with a Thermo VG Scientific ESCALAB 250 spectrometer with a monochromatized Al-Kα X-ray source (1486.6 eV energy). Optical absorption measurements of the composites were performed using a UV–Vis spectrophotometer (Perkin Elmer) in 1 cm cuvettes at range between 200 and 600 nm. A homogeneous suspension in distilled water, obtained through sonication (for 10 min) of well dispersed sample is used for UV–vis studies. The morphology and the particles size were determined by transmission electron microscopy (TEM; Hitachi H-800), and selected area electron diffraction (SAED). The TEM micrographs were taken with an accelerating voltage of 200 kV with samples deposited on a carbon coated copper grid. The wavelength of electron in this condition was approximately about 2.5×10^{-12} m and the camera length was fixed at 170 cm for the selected area electron diffraction. The magnetic measurements were made at room temperature using a vibrating sample magnetometer (VSM) (BHV-55, Riken, Japan).

3 Results and discussion

3.1 XRD studies

The composition of the as-prepared samples was examined by XRD. The XRD pattern of the brown products prepared in alkaline medium (at pH ~ 12) before irradiation is shown in Fig. 1. The results of XRD measurements revealed that all of the refraction peaks can be indexed to a rhombohedral structure of CoO(OH) (JCPDC 14-0673). Some β-$Co(OH)_2$ phase could also be found as trace due to the speed of conversion of $Co(OH)_2$ to $Co(OH)_3$ (and then to CoO(OH)) which is dependent of the alkali concentration. The insert in Fig. 1, provides a typical SEM image of the CoO(OH) sample, illustrating micro sized particles with irregular morphology and some spherical agglomeration of the particles occurred.

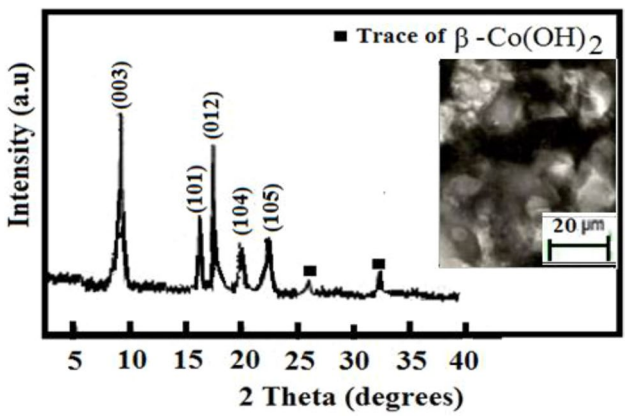

Fig. 1 XRD pattern of cobalt oxyhydroxide, CoO(OH) prepared at pH = 12 before gamma irradiation. The various Bragg peaks are followed by corresponding Miller indices. Results were obtained using CuKα radiation (λ = 1.54178 Å). The transmission electron micrograph, in insert, is of CoO(OH) sol synthesized at room temperature (pH = 12)

The XRD pattern of the black precipitate produced after irradiation is shown in Fig. 2.

All diffraction peaks at 2θ = 19 (111), 31 (220), 37 (311), 39 (222), 45 (400), 56 (422), 59 (511) and 66 (440) displayed on the XRD pattern of the black precipitate produced after gamma irradiation can be indexed to a spinel Co_3O_4 cubic structure (JCPDS No. 43-1003). In this pattern, no peak associated with metal cobalt can be seen, suggesting that the Co_3O_4 is completely pure. On the whole, these diffraction peaks are sharp, narrow and symmetrical with a low and stable baseline, suggesting that the sample is single phased in the cubic crystal structure. Taking into account the fact that the major peak (311) of the interplanar spacing d = 2.41(3) Å, the calculated value of the lattice parameter is about 8.00(3) Å. This value agrees with the one reported in the literature (7.97 Å) [34].

The average size of the Co_3O_4 nanoparticles have been calculated using Debye–Scherrer's equation ($D = 0.92\,\lambda/\beta\cos\theta$), and was found to be about 45 nm. In Scherrer's equation, 0.92 is a constant, λ is the wavelength of the X-rays and β is the full width at half maximum (FWHM) of the diffraction peaks and θ is the diffraction angle.

3.2 SEM and TEM images

The morphology of Co_3O_4 nanoparticles was studied by scanning electron microscope (SEM) and by transmission electron microscope (TEM). The TEM samples were

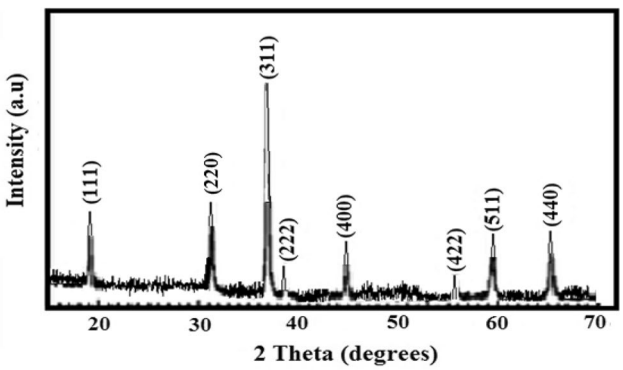

Fig. 2 XRD pattern of Co_3O_4 fabricated at pH = 12 under gamma irradiation. The various Bragg peaks are followed by corresponding Miller indices. Results were obtained using CuKα radiation (λ = 1.54178 Å)

prepared by first dispersing the dried powder constituted of Co_3O_4 particles in alcohol using ultrasonic excitation, then transferring the nanoparticles into the copper grid with carbon support film.

Figure 3a shows the TEM image of the Co_3O_4 nanoparticles. The particles are mostly of spherical shape with a narrow size distribution ranging between 20 and 55 nm and an average size around 45 nm. Some particles are found as agglomerated surface were observed.

It can be seen from this Fig. 3a that there is a uniform distribution of particle size with mean particle size 45.2 nm which is also supported by XRD data.

The SEM image in Fig. 3c reveals that the synthesized Co_3O_4 is consisted of spherical particles with average size of about 45 nm.

Figure 3b shows the electron diffraction micrograph of the prepared material. The lattice spacings corresponding to each ring of diffraction were calculated using the formula $r \times d = L \times \lambda$. The Lλ value was calibrated using the known structure of a polycrystalline gold thin film that was deposited onto an amorphous carbon substrate. The lattice d-spacing from peaks (111), (220), (222), (400), and (511) of the planes causing diffraction were calculated. The calculated d-spacings correspond well to the d-spacings values obtained from the XRD pattern [35, 36]. This indicates furthermore that the sample is Co_3O_4.

Using TEM images, the particle size distribution was plotted in Fig. 4 for the prepared material. The powder has quite narrow size distribution ranged from 20 to 55 nm and an average size around 45 nm. This indicates that particles are seemed to be monodispersed. The particle size calculated from XRD pattern by using the Scherrer formula, and the 100% intensity peak, was about 45 nm, in agreement with the TEM observations.

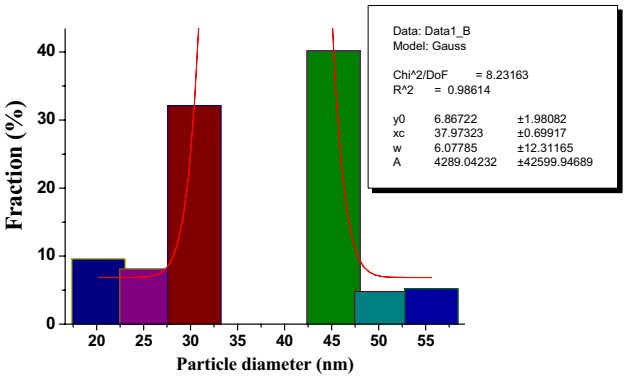

Fig. 4 Particle size distribution of Co_3O_4 nanostructures nanoparticles fabricated under gamma irradiation

3.3 Energy dispersive studies (EDS)

EDS analysis of cobalt oxide nanoparticles was carried out by using internal standard at energy from 0 keV to 10 keV. EDS spectrum (Fig. 5) showed that the synthesized nanopowder has mainly cobalt and oxygen elements and there is small amount of about 3% of carbon detected in the spectrum (due to the polyvinyl alcohol used as caping agent in the preparing Co_3O_4 nanoparticles) [37]. It is confirmed that the cobalt oxide was pure.

The experimental atomic percentages (Fig. 5, the insert) of Co and O are found to be 41.26% and 55.71%, respectively, which is near to the theoretical ratio (3:4) of Co_3O_4. The EDX spectrum supports others characterization techniques.

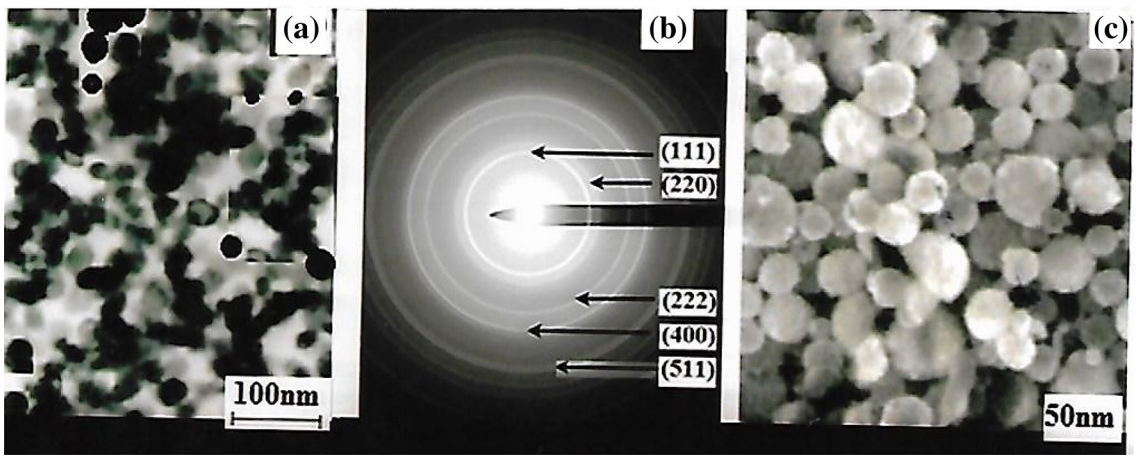

Fig. 3 **a** A low magnification bright field TEM images of Co_3O_4 nanostructures **b** a selected area electron diffraction (SAED) pattern of Co_3O_4 sample **c** The SEM image of Co_3O_4 spinel

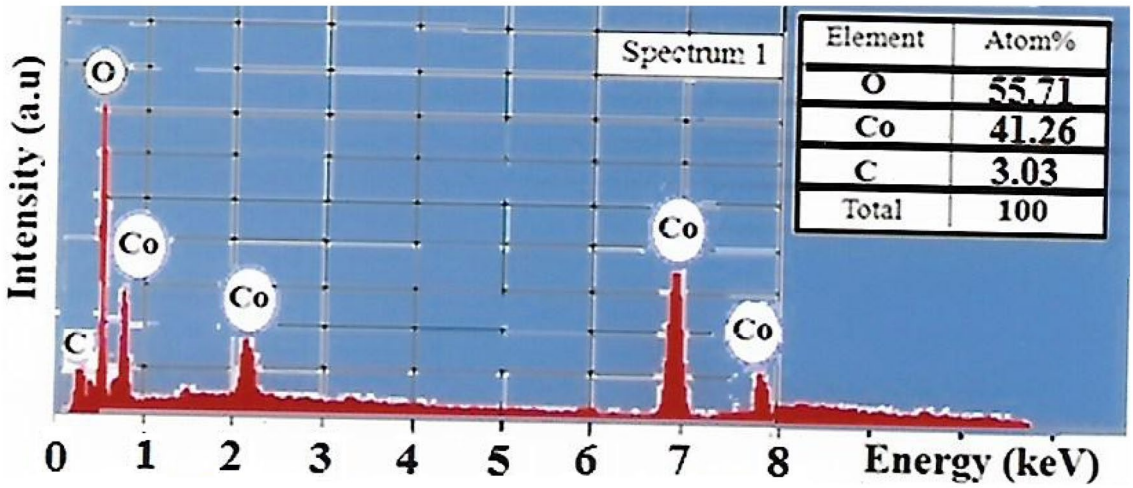

Fig. 5 Energy dispersive X-ray spectrum of Co_3O_4 nanoparticles fabricated under gamma irradiation

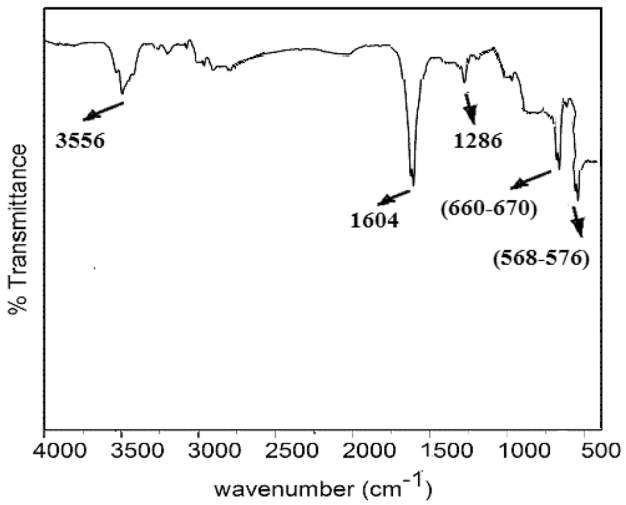

Fig. 6 The FTIR spectrum of Co_3O_4 nanoparticles synthesized under gamma irradiation

3.4 FT- IR spectroscopy analysis

FT- IR spectroscopy (investigated region: 4000–400 cm^{-1}) was carried out in order to ascertain the purity and nature of metal oxide nanopowder. The FT-IR spectrum of as-synthesized Co_3O_4 nanoparticles is indicated in Fig. 6. The spectrum showed significant absorption peaks at about 567–576 cm^{-1} and at about 660–670 cm^{-1}.

The former absorption band at about 660–670 cm^{-1} is attributed to the stretching vibration mode of O–Co–O in which Co is Co^{2+} and is tetrahedrally coordinated. The latter one at 568–576 cm^{-1} can be assigned to Co–O of octahedrally coordinated Co^{3+}. The band which appeared at 3551 cm^{-1} is attributed to OH stretching of the polyvinyl alcohol used as caping agent in the preparing Co_3O_4 nanoparticles and the band located at 1610 cm^{-1} has been assigned binding vibrations of absorbed water molecules on Co_3O_4 nanoparticles [38]. The apparition of these two strong absorption bands provides the clear evidence for the presence of Co_3O_4 spinel oxide crystals [39]. The observed weak band at 1286 cm^{-1} corresponds to $-CH_2-$ bending vibrations from the polyvinyl alcohol used as an organic surfactant in order to stabilize the growth of Co_3O_4 particles during the synthesis.

3.5 XPS analysis

The surface chemical composition of the stoichiometric spinel was studied using X-ray photoelectron spectroscopy.

The XPS spectrum for the fabricated cobalt oxide is shown in Fig. 7, showing characteristic Co 2p peaks shape and binding energies (780 eV and 796 eV) reported for the spinel Co_3O_4 surface.

The O 1s region (peak at 529.6 eV) is consistent with stoichiometric Co_3O_4 single crystal. The main oxygen peak due to lattice O^{2-} is set to 529.6 eV as has been previously found for CoO [40–42] and Co_3O_4 [43–46]. The very weak feature observed at 535.5 eV can be attributed to the lower binding energy shoulder of the Co Auger transition [47, 48].

3.6 Optical measurements

The optical characterization of the as-prepared Co_3O_4 sample was recorded at room temperature on a UV–Visible absorption spectrophotometer. Figure 8 shows

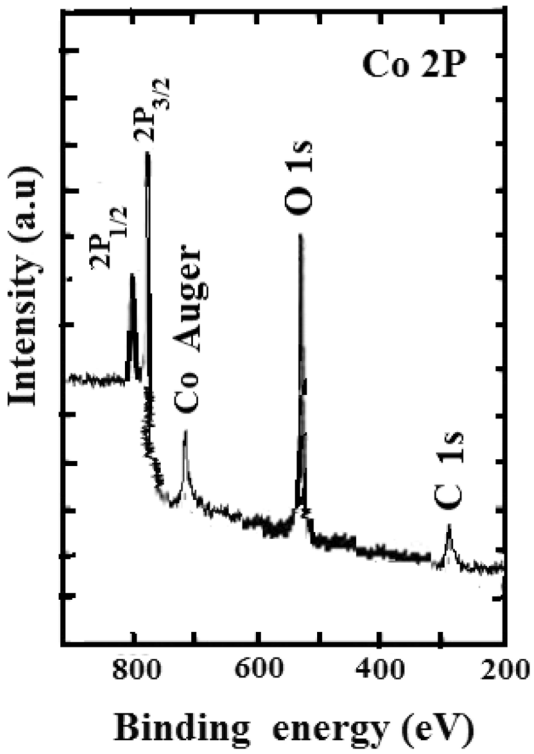

Fig. 7 Survey scan XPS spectrum of Co_3O_4

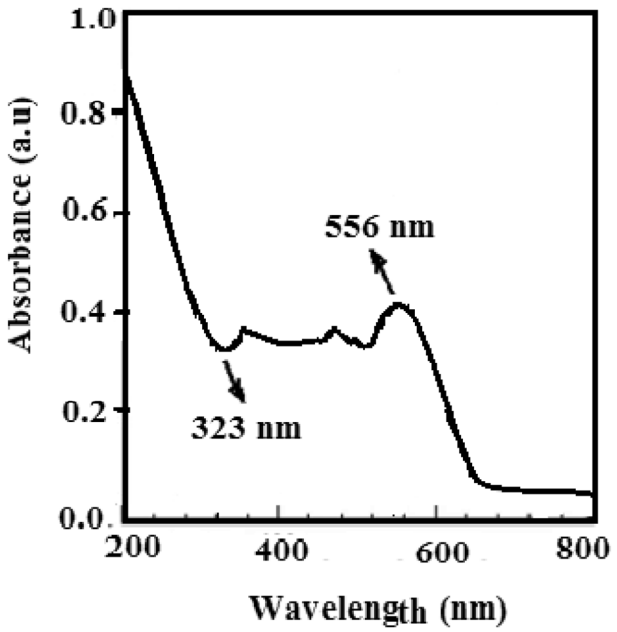

Fig. 8 UV–visible spectrum of cobalt-oxide nanoparticles fabricated under gamma irradiation

UV–Visible spectra of Co_3O_4 nanoparticles as a function of wavelength.

The optical absorption profile shows two absorption bands which appear from 200–370 and 380–600 nm wavelength ranges. The first absorption band can be assigned to the O^{2-} to Co^{2+} charge transfer process, and the second one to the O^{2-} to Co^{3+} charge transfer [49, 50]. These bands are expected for Co_3O_4 [10]. The optical properties of the prepared Co_3O_4 show that the samples exhibited photoabsorption from UV light to visible light region, which implies the possibility of high photocatalytic efficiency of these materials under visible light.

3.7 Magnetic analysis

The magnetic measurements were carried out using Vibrating Sample Magnetometer (VSM) at room temperature. The VSM data of bulk commercial Co_3O_4 shown in Fig. 9a. This is compared with the VSM data of as prepared Co_3O_4 nanoparticles, shown in Fig. 9b.

As shown in Fig. 9a related to the bulk Co_3O_4, the curve exhibits an antiferromagnetic behavior. The bulk Co_3O_4, which is described by a formula unit AB_2O_4 [A: Co^{2+}, B: Co^{3+}] and has a normal spinel structure with antiferromagnetic exchange between Co^{2+} ions which occupy the tetrahedral sites (A) and Co^{3+} ions in octahedral sites (B). Its magnetic moment arises due to Co^{2+} ions largely because of spins. On the other hand, Co^{3+} ions have no permanent magnetic moment. Thus, bulk Co_3O_4 behaves like an antiferromagnetic material.

Although bulk Co_3O_4 shows anti-ferromagnetic behavior, the fine hysteresis loop in Fig. 9b is characteristic of paramagnetic behavior and showed that at 300 K, the saturation magnetization (remanence) of the assembled Co_3O_4 particles is extrapolated to about 0.29 emu g^{-1} at the applied field of 8 kOe, different from the bulk commercial material, which exhibits antiferromagnetic behavior [51, 52].

It is known that the magnetic properties of nanomaterials are shape and size dependent. When the particle size decreases to nanometric scale, the oxygen vacancies occur. Those oxygen vacancies, mainly located on the particle surface, are thought to play a key role for the ferromagnetism behavior in Co_3O_4 nanoparticles. Unpaired electrons can be trapped in those oxygen vacancies and their spins can polarize together via exchange interactions and lead to ferromagnetic order. Thus, we conclude that the change from an antiferromagnetic state for bulk Co_3O_4 to a weakly ferromagnetic state for the Co_3O_4 nanoparticles can be ascribed to the uncompensated surface spins and finite size effects.

These oxides could play a major role in digital data applications. The adopted synthetic route used in the present investigation is expected to be applied in the

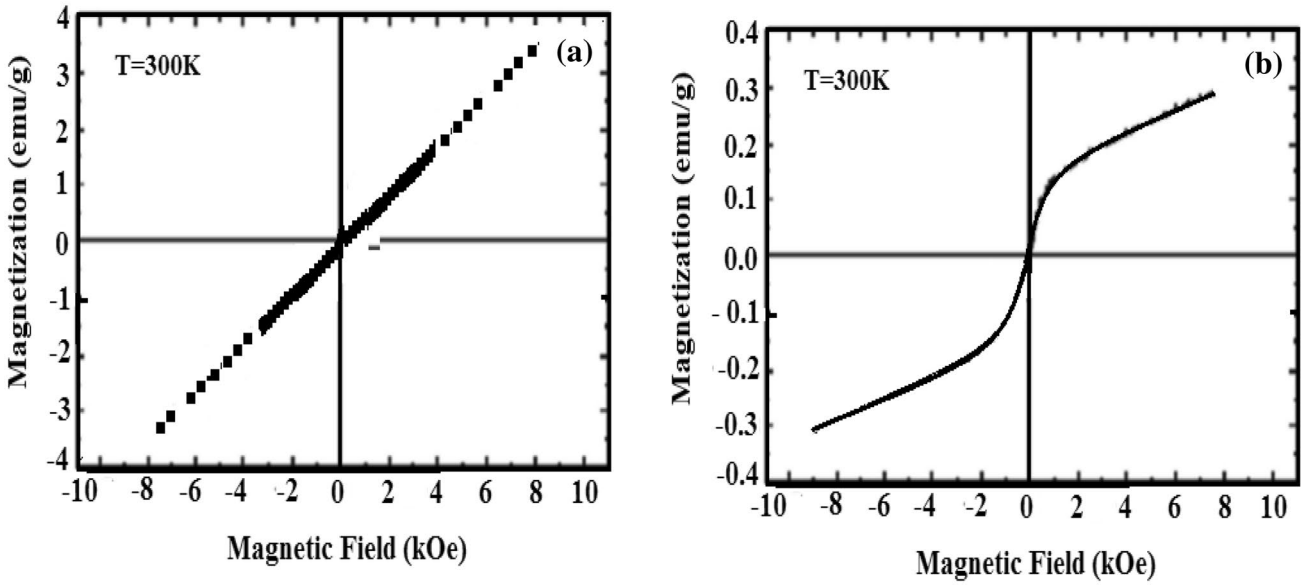

Fig. 9 Magnetization versus APPLIED field graph of **a** bulk Co_3O_4 **b** nanostructures Co_3O_4 prepared at pH 12 by gamma irradiation (30 kGy)

synthesis of other metal oxide semiconductor nanoparticles as building blocks for various nanodevices.

3.8 Mechanism of radiolytic production of Co_3O_4 nanoparticles

From the experiment, the following mechanisms could be suggested to illustrate the formation of Co_3O_4 upon gamma irradiation process.

It is well known that the radiolysis of water produces free radicals such as: e^-_{aq}, $H^{\cdot}$, $HO^{\cdot}$ and $^{\cdot}HO_2$ or $O^{\cdot-}_2$, and molecular products such as H_2 and H_2O_2. It was reported that hydrated electron, e^-_{aq}, and hydrogen radical H· are reducing species, with the standard electrode potentials of e^-_{aq} and H· radical at 25 °C being − 2.77 V and − 2.31 V, respectively; meanwhile, $HO^{\cdot}$, $^{\cdot}HO_2$, $O^{\cdot-}_2$, H_2O_2 are oxidizing species [53, 54]. One can write the following equation:

$$H_2O \xrightarrow{\gamma\text{-}rays} H_2,\ H_2O_2,\ H^{\cdot},\ HO^{\cdot},\ e^-_{aq},\ H_2O^+,\ H_2O^*,\ HO_2 \quad (1)$$

It was observed that, isopropyl alcohol did not totally act as scavenger for oxidative OH· radicals, produced during the radiolysis of water under gamma irradiation

$$(CH_3)_2CHOH + {}^{\cdot}OH \rightarrow (CH_3)_2C^{\cdot}OH + H_2O \quad (2)$$

Some amount of the remained ·OH in the solution could act directly as oxidizing agent (Eq. 4) or could recombined to produce H_2O_2.

$$^{\cdot}OH + {}^{\cdot}OH \rightarrow H_2O_2 \quad (3)$$

Radiation-induced formation of Co_3O_4 nanoparticles requires the presence of stable nucleates of Co^{2+} species $[Co_x(OH)_{2y}^{(x-y)+}]$. Upon exposure to γ-irradiation, the Co^{2+} adsorbed on the nucleates will be quickly oxidized to CoOOH by the oxidizing radiolysis products $HO^{\cdot}$ and H_2O_2, through the reactions [27]:

$$Co^{2+}(sol) + HO^{\cdot} \rightarrow [Co(OH)_3] \rightarrow CoOOH + H_2O \quad (4)$$

The CoOOH then undergoes polycondensation with $Co(OH)_2$ to form Co_3O_4. The conversion of CoOOH to Co_3O_4 is accelerated in the presence of H_2O_2 via reaction (5).

$$6\ CoOOH + H_2O_2 \rightarrow 2\ Co_3O_4 + O_2 + 4\ H_2O \quad (5)$$

4 Conclusion

Spherical sharped particles constituted of supermagnetic Co_3O_4 (with an average size of 45 nm) were prepared successfully by γ-irradiation technique at room temperature, ambient pressure and without any kind of catalysts, in water system. The cobalt oxide nanoparticles were characterized by using XRD, TEM, UV–visible and other characterization tools. The XRD confirms the simple cubic crystal structure of the Co_3O_4. The optical absorption spectrum of cobalt oxide nanoparticles was studied by UV–visible spectroscopy. The mean particle size determined by TEM is in close agreement with the XRD. The present investigation has proven the efficiency of the gamma irradiation in inducing changes in structure and in morphology of the sols prepared before gamma irradiation. The adopted synthetic route is expected to be applied in the synthesis of

other metal oxide semiconductor nanoparticles as building blocks for various nanodevices and as catalysts. The vibrating sample magnetometer (VSM) experiments confirmed the purity, single phase and paramagnetic behavior of the fabricated oxides.

Acknowledgements The authors gratefully thank Dr. Xin Lihui of the National Center of Shanghai Institute of Measurement and Testing Technology for his help with SEM, TEM, Magnetization, FT-IR spectroscopy analysis and XRD analysis, as well as Professor Dr Zhou Ruimin of Shanghai Applied Radiation Institute, Shanghai University, for his support to realize this work.

Compliance with ethical standards

Conflict of interest The authors declare that they have no conflict of interest.

References

1. Xiaoli X, Chao Y, Zhiang L et al (2018) Co-doped CuO nanoarray: an efficient oxygen evolution reaction electrocatalyst with enhanced activity. ACS Substain Chem Eng 6(3):2883–2887
2. Wang Zhe, Sheng jie P, Yuxiang H et al (2017) Cobalt nanoparticles encapsulated in carbon tube-grafted nitrogen and sulfur Co-doped multichannel carbon fibers as efficient bifunctionnal oxygen electrocatalysts. J Mater Chem A 5:4949–4961
3. Lisi X, Xiang R, Qin L et al (2018) A $Ni(OH)_2$–PtO_2 hybrid nanoshet array with ultralow Pt loading toward efficient and durable alkaline hydrogen evolution. J Mater Chem A 6:1967–1970
4. Wei Q, Fan H, Qin F et al (2018) Cathodic electrochemical activation of Co_3O_4 nanoarrays: a smart strategy to significantly boost the hydrogen evolution activity. Chem Comm 54:2150–2153
5. Hui C, Yu-Zhi S, Pan-Yong K et al (2015) Hierarchical $NiCo_2O_4$ nanosheet decorated carbon nanotubes towards highly efficient electrocatalyst for water oxidation. J Mater Chem A 38:19314–19321
6. Yu-Zhi S, Qi-Zhi X, Gao- Feng C et al (2015) One dimensionally Spinel $NiCo_2O_4$ nanowire arrays: facile synthesis, water oxidation and magnetic properties. Electrochim Acta 174:1216–1224
7. Hui C, Chang-Yuan S, Yun Zhi- et al (2017) Interacting $ZnCo_2O_4$ and Au nanodots on carbon nanotubes as efficient water oxidation electrocatalyst. J Power Sources 357:1–10
8. Haiguang Z, Zhiming W, Federico R (2017) Solar cells: highly stable colloidal "giant" quantum dots sensitized solar cells. Adv Funct Met 27(30):17018–17033
9. Sun H, Ahmad M, Zhu J (2013) Morphology controlled synthesis of Co_3O_4 porous nanostructures for the application as lithium-ion battery electrode. Electrochim Acta 89:199–205
10. Makhlouf SA, Bakr ZH, Aly K et al (2013) Structural, electrical and optical properties of Co_3O_4 nanoparticles. Superlattices Microstruct 64:107–117
11. Moon J, Kim TK, Saders BV et al (2015) Black oxide nanoparticles as durable solar absorbing material for high-temperature concentrating solar power system. Sol Energy Mater Sol C 134:417–424
12. Madhu R, Veeramani V, Chen SM et al (2015) Honeycomb-like porous carbon–cobalt oxide nanocomposite for high-performance enzymeless glucose sensor and supercapacitor applications. ACS Appl Mater Interfaces 7(29):15812–15820
13. Cao Y, Yuan F, Yao M et al (2014) A new synthetic route to hollow Co_3O_4 octahedra for supercapacitor applications. Cryst Eng Commun 16:826–833
14. Xu JM, Zhang J, Wang BB et al (2015) Shape regulated synthesis of cobalt oxide and its gas-sensing property. J Alloys Compd 619:361–367
15. Sahoo P, Djieutedjeu H, Poudeu Pierre FP (2013) Co_3O_4 nanostructures: the effect of synthesis conditions on particles size, magnetism and transport properties. J Mater Chem A 1:15022–15030
16. Nandapure BI, Kondawar SB, Nandapure AI (2015) Structural characterization of Co_3O_4 nanoparticles synthesized by a sol–gel method. Int J Sci Res 4(1):440–441
17. Yarestani M, Khalaji AD, Rohani A et al (2004) Hydrothermal synthesis of cobalt oxide nanoparticles: its optical and magnetic properties. J Sci Islamic Republ Iran 25(4):339–343
18. Wadekar KF, Nemade KR, Waghuley SA (2017) Chemical synthesis of cobalt oxide nanoparticles using Co-precipitation method. Res J Chem Sci 7(1):53–55
19. Vijayakumar S, Kiruthika PA, Nagamuthu S et al (2013) Microwave assisted synthesis of Co_3O_4 nanoparticles for high-performance supercapacitors. Electrochim Acta 106:500–505
20. Vidal-Abarca C, Lavela P, Tirado JL (2008) Cobalt oxide nanoparticles prepared from reverse micelles as highcapacity electrode materials for Li-ion cells. Electrochem Solid State Lett 11:A198–A201
21. Kim DY, Ju SH, Koo HY et al (2006) Synthesis of nanosized Co_3O_4 particles by spray pyrolysis. J Alloys Compd 417:254–258
22. Kumar RV, Diamant Y, Gedanken A (2000) Sonochemical synthesis of amorphous Cu and nanocrystalline Cu_2O embedded in a polyaniline matrix. Chem Mater 12:2301–2305
23. Bhatt AS, Bhat DK, Tai C-W et al (2011) Microwave-assisted synthesis and magnetic studies of cobalt oxide nanoparticles. Mater Chem Phys 125:347–350
24. Zou D, Xu C, Luo H et al (2008) Synthesis of Co_3O_4 nanoparticles via an ionic liquid-assisted methodology at room temperature. Mater Lett 62:1976–1978
25. Jiang J, Li L (2007) Synthesis of sphere-like Co_3O_4 nanocrystals via a simple polyol route. Mater Lett 61:4894–4896
26. Fan S, Liu X, Li Y et al (2013) Non-aqueous synthesis of crystalline Co_3O_4 nanoparticles for lithium-ion batteries. Mater Lett 91:291–293
27. Alrehaily LM, Joseph JM, Biesinger MC et al (2013) Gamma-radiolysis-assisted cobalt oxide nanoparticle formation. Phys Chem Chem Phys 15:1014
28. Wren JC (2010) Steady-state radiolysis: effects of dissolved additives, Chap 22. In: ACS symposium, nuclear energy and the environment series. American Chemical Society, Washington, pp 271–295
29. Joseph JM, Choi B-S, Yakabuskie PA et al (2008) A combined experimental and model analysis on the effect of pH and O_2(aq) on γ-radiolytically produced H_2 and H_2O_2. Radiat Phys Chem 77:1009–1020
30. Ekoko BG, Zhou R, Xin LH et al (2006) Effect of pH on the morphology of iron oxides synthesized under gamma irradiation. J Radioanal Nucl Chem 270(2):473–478
31. Zhang X, Zhou R, Rao W et al (2006) Influence of precipitor agents NaOH and NH_4OH on the preparation of Fe_2O_3 nanoparticles synthesized by electron beam irradiation. J Radioanal Nucl Chem 270(2):285–289
32. Ekoko Bakambo G, Lobo Joseph K-K, Mvele Omer M et al (2014) Gamma irradiation inducing the synthesis of magnetic Fe_3O_4 nanorod particles in alkaline medium. Int J Mater Sci Appl 3(6):339–343
33. Baes CF, Mesmer RS, Krieger RE (1986) Hydrolysis of cations. Wiley, New York

34. Al-Tuwirqi R, Al-Ghamdia AA, Aal NA et al (2011) Facile synthesis and optical properties of Co_3O_4 nanostructures by the microwave route. Superlattices Microstruct 49(4):416–421
35. Long NV, Ohtaki M, Hien TD et al (2011) Synthesis and characterization of polyhedral and quasi-sphere non-polyhedral Pt nanoparticles: Effects of their various surface morphologies and sizes on electrocatalytic activity for fuel cell applications. J Nanopart Res 13(10):5177–5191
36. Williams DB, Carter CB (2009) Transmission electron microscopy. A textbook for materials science. Springer, Berlin
37. Surekha SJ, Abhishek D, Dhayagude A et al (2015) Role of PVA in synthesis of nano Co_3O_4 decorated graphene. Polym Adv Technol 26:9
38. Teng Y, Yamamoto S, Kusano Y et al (2010) One-pot hydrothermal synthesis of uniformly cubic Co_3O_4 nanocrystals. Mater Lett 64:239–242
39. Lester E, Aksomaityte G, Li J et al (2012) Controlled continuous hydrothermal synthesis of cobalt oxide (Co_3O_4) nanoparticles. Prog Cryst Growth Charact Mater 58:3–13
40. Carson GA, Nassir MH, Langell MA (1996) Epitaxial growth of Co_3O_4 on CoO (100). J Vac Sci Technol A 14:1637
41. Langell MA, Carson GA, Smith S et al (1999) The valence electronic structure of Co_3O_4: is it a charge-transfer insulator? Mater Res Soc Symp Proc 547:255
42. Jimenez VM, Fernadez A, Espinos JP et al (1995) The state of the oxygen at the surface of polycrystalline cobalt oxide. J Electron Spectrosc Relat Phenom 71:61–71
43. Gautier JL, Rios R, Garcia M et al (1997) Characterization by X-ray photoelectron spectroscopy of thin $Mn_xCo_{3-x}O_4(1 \geq x \geq 0)$ spinel films prepared by low-temperature spray pyrolysis. Thin Solid Films 311:51
44. Carson GA, Nassir MH, Langell MA (1998) CoO(100) and CoO(100)/Co_3O_4 Fuchs–Kliewer phonon spectra. Surf Sci Spectra 5:235
45. Langell MA, Carson GA, Anderson M et al (1999) Valence-band electronic structure of Co_3O_4 epitaxy on CoO(100). Phys Rev B 59:4791
46. Wang D, Chen X, Evans DG et al (2013) Well-dispersed Co_3O_4/Co_2MnO_4 nanocomposites as a synergistic bifunctional catalyst for oxygen reduction and oxygen evolution reactions. Nanoscale 5:5312–5315
47. Wagner CD, Riggs WM, Davis L et al (1979) Handbook of X-ray photoelectron spectroscopy. Physical Electronics Industries, Perkin Elmer, Eden Prairie
48. Sarah CP, Erin MM, Gregory AC et al (2008) Cobalt oxide surface chemistry: the interaction of CoO (100), Co_3O_4 (110) and Co_3O_4 (111) with oxygen and water. J Mol Catal A Chem 281(1–2):49–50
49. Sun L, Li H, Ren L et al (2009) Synthesis of Co_3O_4 nanostructures using a solvothermal approach. Solid State Sci 11:108–112
50. Gu F, Li C, Hu Y et al (2007) Synthesis and optical characterization of Co_3O_4 nanocrystals. J Cryst Growth 304:369–373
51. Farhadi S, Safabakhsh J, Zaringhadam P (2012) Synthesis, characterization, and investigation of optical and magnetic properties of cobalt oxide (Co_3O_4) nanoparticles. J Nanostruct Chem 3:69
52. Yarestani M, Khalaji AD, Rohani A et al (2014) Hydrothermal synthesis of cobalt oxide nanoparticles: its optical and magnetic properties. J Sci Islamic Republ Iran 25(4):339–343
53. Buxton GV, Greenstock CL, Helman WP et al (1988) Critical review of rate constants for reactions of hydrated electrons, hydrogen atoms, and hydroxyl radicals ($\cdot OH/\cdot O^-$) in aqueous solution. J Phys Chem Ref Data 17:513–886
54. Spinks JWT, Woods RJ (1990) An Introduction to radiation chemistry, 3rd edn. Wiley, New York, p 285